INMM and ESARDA 2023

Exploration of Morphologic Signatures of Uranium Tetrafluoride for Nuclear Forensic Science

Alexa Hanson [1], Ian Schwerdt [2], Kathleen Matthies [2], Cole Thompson [3], Kari Sentz [4]

[1] Material Physics and Applications Division, Los Alamos National Laboratory, Los Alamos, NM, USA
[2] Intelligence and Systems Analysis Division, Los Alamos National Laboratory, Los Alamos, NM, USA
[3] Radiation Transport Applications Division, Los Alamos National Laboratory, Los Alamos, NM, USA
[4] Information Sciences Division, Los Alamos National Laboratory, Los Alamos, NM, USA

alexah@lanl.gov

ABSTRACT

UF_4 is a common feedstock for production of uranium metal and UF_6, and open-source publications regarding the morphology of UF_4 are limited. Current research has quantitatively demonstrated the utility of uranium oxide morphology to identify experimental variables such as precipitation conditions, thermal history, and storage conditions, among others. We hypothesize similar signatures will be observable in uranium fluorides. Thus, this study investigates morphologic synthetic pathway signatures of UF_4 from the ammonium bicarbonate (AUC) and ammonium diuranate (ADU) precipitation routes. Experimentation is ongoing. To develop these signatures, UO_2 will be synthesized from both AUC and ADU precipitates, which have largely differing surface areas and morphologies. The UO_2 from each synthetic route will be fluorinated using ammonium bifluoride in a fluidized bed reactor to form UF_4. Powder X-ray diffraction will be used to confirm the phase purity of the reaction product, while scanning electron microscopy in conjunction with Morphological Analysis of Materials (MAMA) software will be utilized to quantify the material morphology. Additionally, a custom four-factor response surface model design of experiment (DOE) will be used to interpolate between various factors of the fluorination and resulting morphology. Quantifying these material attributes of UF_4 is relevant to the morphologic signature for nuclear forensic analyses and nuclear fuels production.

INTRODUCTION

From 1993-2022, there were over 500 confirmed cases of nuclear material interdicted outside of regulatory control.[1] With the possibility of these incidents being linked to illicit trafficking or malicious use, there is a critical need to develop forensics signatures to determine where and how a sample of nuclear material was synthesized. Corresponding to the complexity of nuclear materials synthesis, there are numerous factors that can contribute to unique forensic signatures. For example, in UO_2 production, parameters such as uranium ore processing purities, precipitation conditions, calcination temperatures and durations, storage conditions and others, often vary between facilities. Each of these parameters may influence the physical and chemical properties of the nuclear sample. There are many forensic techniques for analysis that provide varying degrees of insight and information to identify and characterize such material. One emerging signature is particle morphology, which has demonstrated the ability to quantitatively characterize experimental design parameters [2-5]. Morphological signatures for nuclear forensics is a focus of new research and development efforts in the National Nuclear Security Administration (NNSA).[6]

LA-UR-23-25342

Morphologic signatures are particularly useful in scenarios where other analytical techniques may not provide enough information for discerning process history. For example, X-ray diffraction (XRD) provides data regarding the crystal structure of materials and can readily be used to distinguish between various crystalline uranium oxide species. Nevertheless, if a sample set contains uranium oxides synthesized from varying uranium ore concentrates (UOCs), for example: UO_3 synthesized from both uranyl peroxide and sodium diuranate, XRD alone cannot elucidate which synthetic pathway was used. However, similarly to the aforesaid parameters, synthetic route has been empirically demonstrated to have a quantitative effect on particle morphology, and thus, could be used to discern between pathways.[7] In this manner, morphologic signatures provide complementary information to traditional nuclear forensic techniques.

Of particular interest in this work is the morphology of uranium tetrafluoride, UF_4, which is a common feedstock in producing UF_6 and uranium metal. Previous work has reported qualitative scanning electron microscopy (SEM) imagery illustrating the particle morphology of commercially purchased anhydrous UF_4 [8, 9] and UF_4 produced from UO_2F_2 with hydrofluoric acid, HF, used as the precipitating agent and $SnCl_2$ as the reducing agent.[10, 11] However, to our knowledge, there have been no quantitative studies regarding UF_4 morphology. Quantitative morphological analysis can provide statistical features for characterizing materials, thus decreasing the potential for user bias in qualitatively describing the particle morphology and enabling the potential for a morphologic database for sample characterization. We anticipate that quantitatively distinguishing morphological signatures of uranium oxides (*vide supra*) will also be applicable to uranium fluoride species. Therefore, this ongoing work investigates the morphologic signatures of UF_4 produced with ammonium bifluoride (ABF) and UO_2 synthesized from two common UOC precipitation routes, ammonium diuranate (ADU), shown in Equation 1 and ammonium uranyl carbonate (AUC), shown in Equation 2.

$$2UO_2(NO_3)_2 + 6NH_4OH \rightarrow (NH_4)_2U_2O_7 + 4NH_4NO_3 + 3H_2O \quad (1)$$

$$UO_2(NO_3)_2 + 3(NH_4)_2CO_3 \rightarrow (NH_4)_4[UO_2(CO_3)_3] + 2NH_4NO_3 \quad (2)$$

Following reduction to UO_2, samples will be converted to UF_4 precursor $(NH4)_4UF_8$ with ABF at varying molar excesses. This intermediate material reaction occurs as follows[12]:

$$UO_2 + 4NH_4HF_2 \rightarrow (NH_4)_4UF_8 \cdot 2H_2O \quad (3)$$

$(NH4)_4UF_8$ samples will then be heated to form UF_4 under varying conversion temperatures as outlined in Equation 4.[12] The synthetic conditions used for UF_4 formation were based on a custom four-factor design of experiment (DOE) discussed in the following section. We anticipate the varying molar excesses of ABF:UO_2 and conversion temperatures will quantitatively affect the final UF_4 morphology.

$$(NH_4)_4UF_8 \rightarrow UF_4 + 4NH_3 + 4HF \quad (4)$$

For material characterization, XRD was used to confirm the phase purity of the AUC and ADU precipitates. While experimentation remains ongoing, UF_4 materials will undergo similar analyses. Similarly, SEM in conjunction with Morphological Analysis of MAterials (MAMA) software will

be used to quantify the particle morphology. A response surface model illustrating the effect of starting material, ABF:UO_2 molar excess, and initial and final UF_4 conversion temperatures on the UF_4 morphology will be presented.

MATERIALS AND METHODS

Design of Experiment (DOE)

The DOE was modelled in JMP utilizing a custom four-factor design.[13] The starting materials ADU and AUC represent a categorical variable, whereas the remaining three continuous experimental variables are molar excess of ABF:UO_2, initial conversion temperature, and final conversion temperature. The range of values for each continuous variable was chosen based on a compilation of previously reported experimental methods for a total of 20 runs.[12, 14-18] The molar excess of ABF:UO_2 will range from 10-40%; the initial conversion temperatures for Equation 3will range from 110-150°C; and the final conversion temperature for Equation 4 will range from 400-550°C. Resulting quantitatively distinguishable responses are anticipated to include UF_4 content (wt %) and morphological attributes such as particle pixel area, circularity, and ellipse aspect ratio, which are discussed in more detail in the following section.

Material Syntheses

Synthesis of the ADU starting material was adapted from a range of previously reported experimental conditions.[19-22] Uranyl nitrate hexahydrate (UNH), $UO_2(NO_3)_2{\cdot}6H_2O$, was dissolved in deionized water to form a 50 g·U/L solution. Ammonium hydroxide, NH_4OH, was added dropwise to the UNH solution at 50°C and 400 rpm until a pH of 7.5 was reached. The resulting solution was allowed to digest for one hour, then filtered and washed thrice with 50 mL of deionized water to remove residual impurities. The washed ADU was dried under ambient conditions for 24 hours, then dried in a muffle furnace at 100°C for an additional 24 hours.

The synthetic procedure for the AUC starting material was developed from Sadeghi et al.[23] A 100 mL 75 g·U/L UNH solution, 200 mL 600 g/L ammonium bicarbonate solution, NH_4HCO_3, and 110 mL 500 g/L ammonium carbonate solution, $(NH_4)_2CO_3$, prepared through the addition of ammonium bicarbonate into ammonium hydroxide, were heated to 60°C at 400 rpm. Following temperature equilibration, the entirety of the heated UNH solution was added dropwise to the heated ammonium bicarbonate solution. The ammonium carbonate solution was then added dropwise to the resulting solution and allowed to digest for 2.5 hours. The final pH of the solution was 9.19. The AUC was filtered and washed with 50 mL of methanol and dried under ambient conditions for 72 hours.

To form UO_2, the ADU and AUC starting materials will be calcined for 20 hours at 800°C under 150 mL/min of argon gas, cooled to ambient temperature, then reduced at 550°C for 8 hours under 150 mL/min of forming gas. Preliminary tests have been conducted to verify the calcination and subsequent reduction methods.

To produce UF_4, UO_2 will first be mixed with ABF, NH_4HF_2, to produce intermediate material $(NH4)_4UF_8$. The ABF will be mixed with UO_2 at varying degrees of molar excesses as outlined by

the DOE. UF_4 will then be synthesized via the heating of NH_4UF_8 in a fluidized bed reactor. A schematic of the fluidized bed reactor is depicted in Figure 1. The reactions will be conducted under argon at 1 standard cubic foot per hour (SCFH). The system is comprised of ⅛" stainless steel gas lines, and the bed itself is ½" Inconel tubing. The gas line inlet is fitted with a high-capacity oxygen and moisture trap, while the bed is fitted with heat tape for temperature control and ceramic fiber insulation. Valves are incorporated to isolate the oxygen scrubber and bed between runs. Following Equation 4, the offgas is expected to be comprised of argon, hydrofluoric acid, water, and ammonia, which will be neutralized via KOH solution. The fluidized bed reactor has been assembled and test runs are under way.

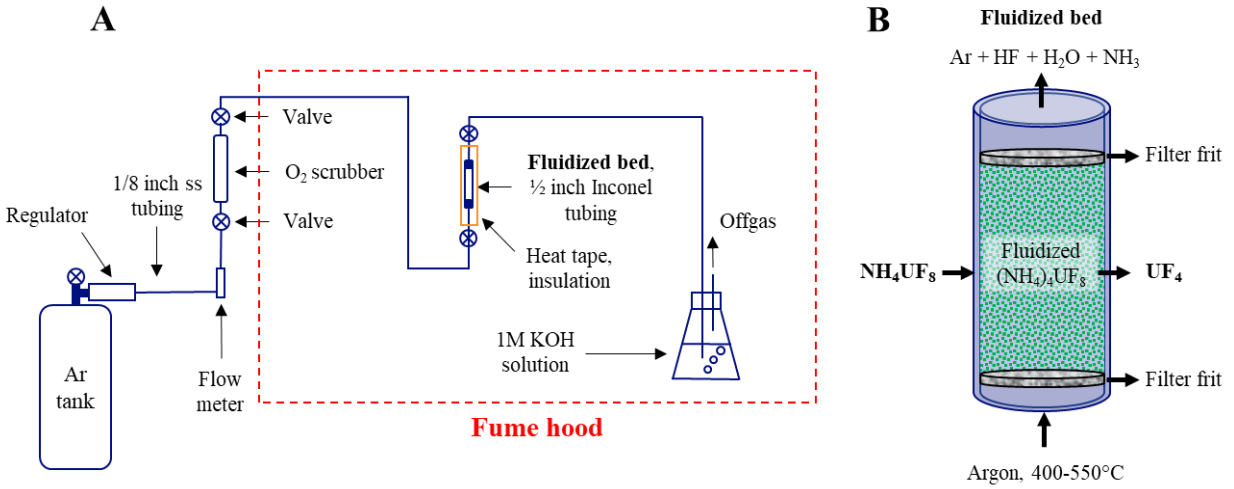

Figure 1. (a) Schematic illustrating the fluidized bed reactor assembly. UO_2 will be mixed with ABF to form intermediate material $(NH_4)_4UF_8$, which will be heated under argon with varying conversion temperatures to form UF_4. (b) More detailed schematic of the fluidized bed constituents depicted in (a).

ANALYTICAL METHODS AND PRELIMINARY RESULTS

Powder X-ray Diffraction (p-XRD)

P-XRD was used to confirm the phase purity of the ADU and AUC. Scans were collected on a Bruker D8 Advance diffractometer with an unconditioned copper source and 1-D Si(Li) Lynxeye detector. The scans were conducted at 6 seconds per step with a 0.02° increment and PSD opening of 3.03° from 10 to 70° 2θ. Samples were sealed in Bruker airtight holders to mitigate particulate dispersion and were rotated at 15 rpm to account for any preferred orientation. As depicted in Figure 2 the ADU precipitate had the stoichiometry $2UO_3 \cdot NH_3 \cdot 3H_2O$, which has been observed in prior work and is likely attributed to the pH>7 precipitation.[24] The AUC precipitate was identified as $(NH_4)_4(UO_2(CO_3)_3$ as expected. The resulting spectra did not indicate any minor component phases in either starting material. P-XRD will additionally be utilized to determine the phase composition of the UF_4 samples.

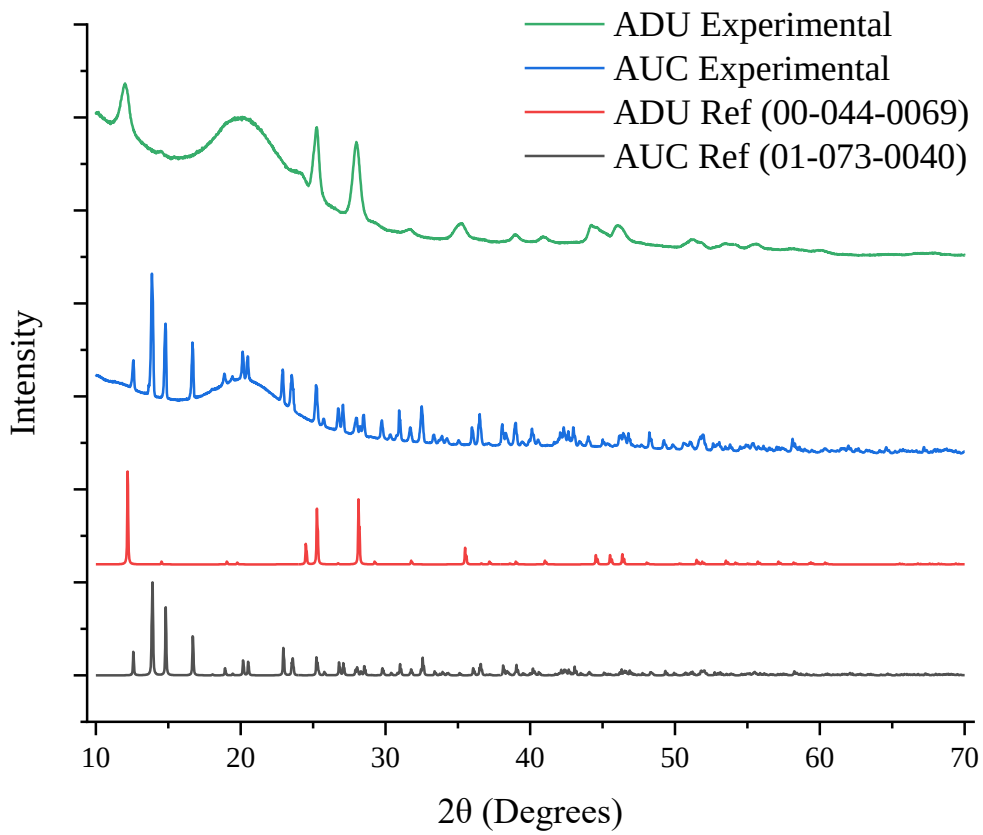

Figure 2. XRD patterns for the ADU and AUC starting material shown in green and blue, respectively. The amorphous structure is attributed to the sample holders. The corresponding reference patterns for ADU (PDF 00-044-0069) and AUC (01-073-0040) are shown in red and black. Peak intensities were normalized for comparative purposes.

Scanning Electron Microscopy (SEM)

SEM was utilized to investigate the starting material morphology. Samples were prepared by dusting a few milligrams of material onto a 12 mm adhesive carbon tab adhered to a 12.7 mm aluminium pin stub mount. The images were collected on a FEI Quanta 200F field emission SEM using a 20 kV accelerating voltage, 10 mm working distance, and an Everhart-Thornley detector. Magnifications were varied to highlight various aspects of the material morphology. Figure 3 compares imagery of the ADU and AUC samples at 10,000x magnification, where the AUC was observed to have a much larger, blocky particle morphology compared to the ADU at the same magnification, as projected by previous work.[7] These differing starting material morphologies are anticipated to quantitatively affect the final UF_4 morphology.

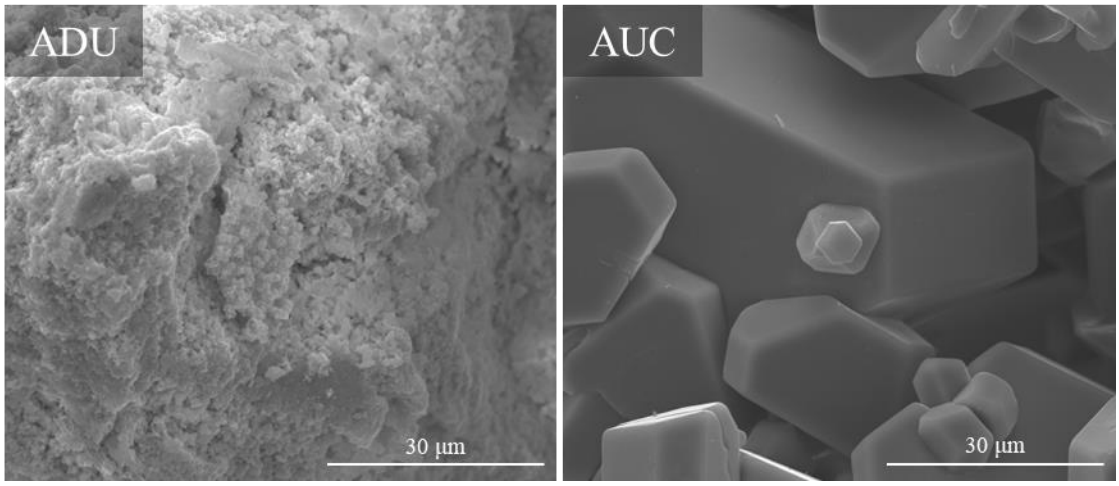

Figure 3. SEM-SE images comparing starting materials ADU and AUC at 10,000x magnification.

Quantitative Morphological Analysis

In conjunction with the SEM imagery, particle segmentation in MAMA software is being utilized to quantify the material morphology. Segmentation criterion was built upon that described by Olsen et al., and requires the particle to have clear, distinct boundaries, not be obstructed by the image frame or occluded by overlapping particles, and of adequate pixel size to represent the true shape of the particle (>100 pixel^2).[25] The segmented particle dataset will be characterized according to the following attributes: pixel area, ellipse aspect ratio, circularity, perimeter convexity, area convexity, and diameter aspect ratio, which are common robust size attributes and have been verified to give accurate resolution in the MAMA software.[26, 27] Figures 4 and 5 compare SEM imagery of ADU and AUC particles before and after segmentation in MAMA. The ADU starting material consists of distinct, rounded micro particles, while the blocky AUC micro particles appear fused together. As such, the AUC macro particle morphology (defined here as clusters of micro particles) is being segmented, as opposed to the micro particle morphology for ADU. Segmentation and subsequent statistical analyses are in progress and will additionally be applied to the UF_4 particle morphology.

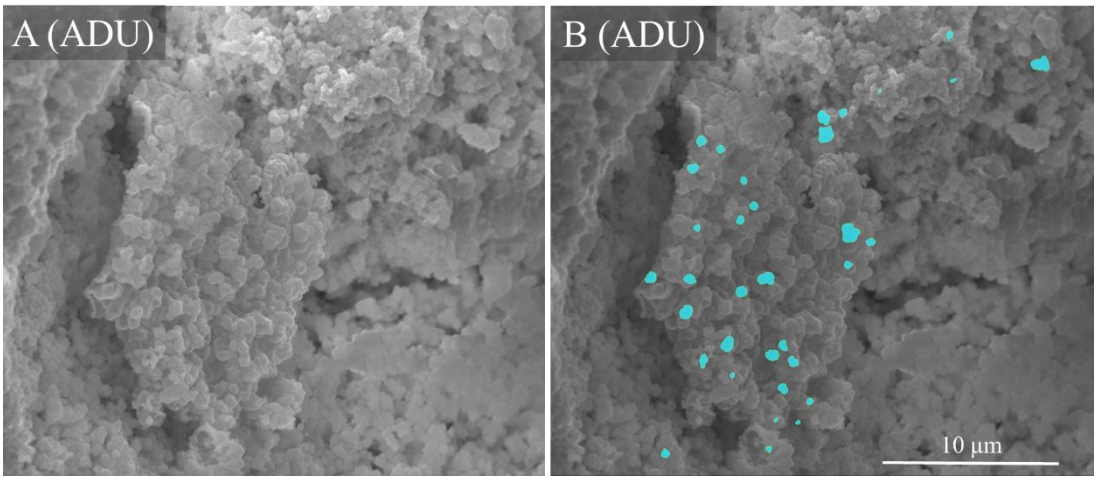

Figure 4. SEM Images of A) ADU starting material at 25,000x prior to MAMA segmentation; B) ADU starting material at 25,000x following micro particle segmentation.

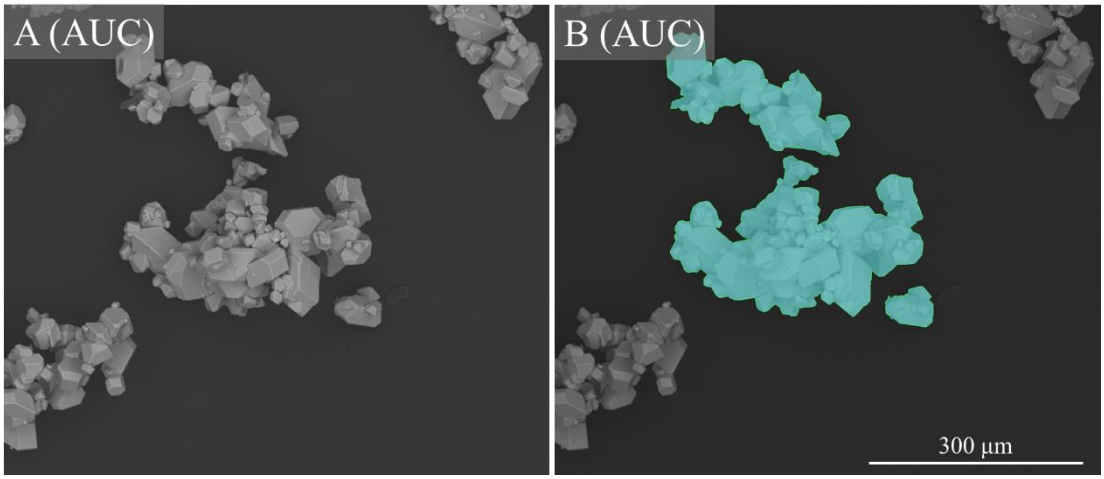

Figure 5. SEM Images of A) AUC starting material at 1000x prior to MAMA segmentation; B) AUC starting material at 1000x following macro particle segmentation. The micro particles appear fused together and could not be individually segmented.

CONCLUSIONS

In this study, UF_4 will be synthesized via ABF and UO_2 precipitated from ADU and AUC. While experimentation is ongoing, P-XRD will ultimately be utilized to determine UF_4 content following each conversion. Further, SEM in conjunction with quantitative analysis via MAMA will elucidate the morphological effects of ADU versus AUC precipitation routes, ABF:UO_2 molar ratio, and initial and final conversion temperatures on UF_4. Predictive profiling via the response surface model DOE will determine which factor has the most statistically relevant morphological impact. This work is an important advancement to the understanding of the morphological properties of UF_4 under varying synthetic conditions and marks the first contribution to a quantitative U-fluorides morphological dataset. These advancements will provide the nuclear forensics and nonproliferation community with deeper insights and expand the reference material for determining material process history through morphological characterization.

ACKNOWLEDGEMENTS

This work is supported by the U.S. Department of Energy National Nuclear Security Administration Office of Defense Nuclear Nonproliferation Research and Development under grant no. LA21-ML-MorphologySignature-P86-NTNF1b. The views and conclusions contained in this document are those of the authors and should not be interpreted as necessarily representing the official policies, either expressed or implied, of the U.S. Department of Energy.

REFERENCES

1. IAEA. *IAEA Incident and Trafficking Database (ITDB) 2023 Factsheet*. 2023.
2. Nizinski, C., et al., *Effects of process history on the surface morphology of uranium ore concentrates extracted from ore.* Accepted to Minerals Engineering, 2020.
3. Olsen, A.M., et al., *Quantification of high temperature oxidation of U_3O_8 and UO_2.* Journal of Nuclear Materials, 2018. **508**: p. 574-582.
4. Abbott, E.C., et al., *Dependence of UO2 surface morphology on processing history within a single synthetic route.* Radiochimica Acta, 2019. **107**: p. 1121-1131.
5. Hanson, A.B., et al., *Impact of Controlled Storage Conditions on the Hydrolysis and Surface Morphology of Amorphous-UO_3.* ACS Omega, 2021. **6**: p. 8605-8615.
6. Eppich, G.R. *New CRP: Nuclear Forensics Science to Strengthen the Connection Between the Radiological Crime Scene and the Nuclear Forensics Laboratory (J02020)*. 2022.
7. Schwerdt, I.J., et al., *Uranium oxide synthetic pathway discernment through thermal decomposition and morphological analysis.* Radiochimica Acta, 2018. **107**: p. 193-205.
8. Christian, J.H., et al., *Characterizing the solid hydrolysis product, $UF_4(H_2O)_{2.5}$, generated from neat water reactions with UF_4 at room temperature.* Dalton Trans, 2021. **50**(7): p. 2462-2471.
9. Foley, B.J., et al., *Probing the hydrolytic degradation of UF(4) in humid air.* Dalton Trans, 2022. **51**(15): p. 6061-6067.
10. Durazzo, M., et al., *Analysis of Slag Formation During UF_4 Magnesiothermic Reduction.* Nuclear Technology, 2017. **200**(2): p. 170-176.
11. Durazzo, M., et al., *Manufacturing Low Enriched Uranium Metal by Magnesiothermic Reduction of UF_4.* Annals of Nuclear Energy, 2017. **110**: p. 874-885.
12. Wani, B.N.P., S. J.; Rao, U.R.K.; Venkateswarlu, K.S., *Fluorination of Oxides of Uranium and Thorium by Ammonium Hydrogen Fluoride.* Journal of Fluorine Chemistry, 1988. **44**: p. 177-185.
13. Inc., S.I., *JMP® Pro Version 17.0.0*. Cary, NC.
14. Claux, B., et al., *On the fluorination of plutonium dioxide by ammonium hydrogen fluoride.* Journal of Fluorine Chemistry, 2016. **183**: p. 10-13.
15. Crocker, H.W., *Ammonium Bifluoride Fusion of Ignited Plutonium Dioxide*, in *234-5 Development Operation Research and Engineering Operation Chemical Processing Department*. 1961, Atomic Energy Commission under General Electric: Hanford Atomic Products Operation.
16. Silva Neto, J.B., et al., *Production of uranium tetrafluoride from the effluent generated in the reconversion via ammonium uranyl carbonate.* Nuclear Engineering and Technology, 2017. **49**(8): p. 1711-1716.

17. Tolley, W.B., *The Preparation of Plutonium (IV) Ammonium Fluoride and its Decomposition to Plutonium Tetrafluoride for Subsequent Reduction to Metal*, in *Metallurgy Unit Applied Research Sub-Section*. 1954, Atomic Energy Commission under General Electric: Hanford Atomic Products Operation.
18. Yeamans, C.B., *Synthesis of Uranium Fluorides from Uranium Dioxide with Ammonium Bifluoride and Ammonolysis of Uranium Fluorides to Uranium Nitrides*, in *Nuclear Engineering*. 2008, University of California, Berkeley. p. 131.
19. Ainscough, J.B. and B.W. Oldfield, *Effect of ammonium diuranate precipitation conditions on the characteristics and sintering behaviour of uranium dioxide.* Journal of Applied Chemistry, 2007. **12**(9): p. 418-424.
20. Eloirdi, R., et al., *Investigation of ammonium diuranate calcination with high-temperature X-ray diffraction.* Journal of Materials Science, 2014. **49**(24): p. 8436-8443.
21. Manna, S., et al., *Study on effect of process parameters and mixing on morphology of ammonium diuranate.* Journal of Radioanalytical and Nuclear Chemistry, 2016. **310**: p. 287-299.
22. Rajagopal, S.A., T. P. S.; Iyer, C. S. P., *Particle size analysis of ammonium uranate prepared by conventional and homogeneous methods of precipitation and their corresponding oxides.* Journal of Nuclear Materials, 1996. **227**: p. 300-303.
23. Sadeghi, M.H., M. Outokesh, and M.H. Zare, *Production of high quality ammonium uranyl carbonate from "uranyl nitrate + carbonate" precursor solution.* Progress in Nuclear Energy, 2020. **122**.
24. Cordfunke, E.H.P., *On the Uranates of Ammonium-I. The Ternary System NH_3-UO_3-H_2O.* Journal of Inorganic Nuclear Chemistry, 1962. **24**: p. 303-307.
25. Olsen, A.M., et al., *Quantifying Morphological Features of α-U_3O_8 with Image Analysis for Nuclear Forensics.* Analytical Chemistry, 2017. **89**: p. 3177-3183.
26. Porter, R.B. and C.E. Ruggiero. *LA-UR-14-23625. MAMA Software Features: Quanification Verification Documentation-1*. 2014.
27. Ruggiero, C.E. and R.B. Porter. *LA-UR-14-23579. MAMA Software Features: Quantified Attributes*. 2014.